To cite this version :

Flow Structure Oscillations and Tone Production in Underexpanded Impinging Round Jets

Romain Gojon* and Christophe Bogey†

Université de Lyon, Ecole Centrale de Lyon, 69134 Ecully, France

Flow structure oscillations and tone generation mechanisms in an underexpanded round jet impinging on a flat plate normally have been investigated using compressible large-eddy simulations. At the exit of a pipe nozzle of diameter D, the jet is characterized by a nozzle pressure ratio of 4.03, an exit Mach number of 1, a fully expanded Mach number of 1.56, and a Reynolds number of 6×10^4. Four distances between the nozzle and the plate of $2.08D$, $2.80D$, $3.65D$, and $4.66D$ are considered. Snapshots of vorticity, density, pressure, and mean velocity flowfields are first presented. The latter results compare well with data of the literature. In three cases, in particular, a Mach disk appears to form just upstream from the plate. The convection velocity of flow structures between the nozzle and the plate, and its dependence on the nozzle-to-plate distance, are then examined. The properties of the jet near pressure fields are subsequently described using Fourier analysis. Tones emerge in the spectra at frequencies consistent with those expected for an aeroacoustic feedback loop between the nozzle and the plate as well as with measurements. Their amplitudes are particularly high in the presence of a near-wall Mach disk. The axisymmetric or helical natures of the jet oscillations at the tone frequencies are determined. The motions of the Mach disk found just upstream from the plate for certain nozzle-to-plate distances are then explored. As noted for the jet oscillations, axially pulsing and helical motions are observed, in agreement with experiments. Finally, the intermittency of the tone intensities is studied. They significantly vary in time, except for the two cases where the near-wall Mach disk has a nearly periodic motion at the dominant tone frequency.

I. Introduction

FOR high subsonic and supersonic jets impinging on a flat plate normally, very intense tones have been measured in the acoustic field by Powell [1] and Wagner [2], among others. In particular, a staging phenomenon of the main tone frequency has been observed as the distance between the jet nozzle and the flat plate varies. Therefore, Powell [1] suggested that the tones are generated by a feedback loop between the jet nozzle and the flat plate, involving the turbulent structures propagating downstream and the acoustic waves propagating upstream. Such a self-sustaining oscillating flow can be encountered in a variety of configurations where a free shear layer impinges on a solid boundary, as reported by Rockwell and Naudasher [3] and Rockwell [4].

The tone frequencies in subsonic impinging round jets can be predicted by the feedback mechanism model formulated by Ho and Nosseir [5] and Nosseir and Ho [6]. Another model was proposed by Tam and Ahuja [7], in which the upstream-propagating waves of the feedback mechanism are associated with neutral acoustic wave modes of the vortex sheet model of the jets. The model provided an allowable frequency range for each of these modes, in which the tone frequencies measured by Wagner [2] for high subsonic round jets were found to lie.

Supersonic round jets impinging on a flat plate normally have been investigated experimentally by Henderson and Powell [8], Krothapalli et al. [9], and Henderson et al. [10], for instance. In some cases, a feedback mechanism is observed as in subsonic jets. This is very often the case when the jets are ideally expanded, but this happens only for some nozzle-to-plate distances when the jets are imperfectly expanded. Henderson and Powell [8] suggested that, in the latter case,

the feedback loop establishes only when a Mach disk forms just upstream from the plate. As shown by Krothapalli et al. [9], there can be recirculation zones between this Mach disk and the flat plate for some nozzle-to-plate distances. More recently, Risborg and Soria [11] explored the instability modes of underexpanded impinging jets using ultra-high-speed schlieren and shadowgraphy techniques. Axial and helical modes were identified, and the Mach disk located just upstream from the plate was found to oscillate. For similar jets, Buchmann et al. [12] noted the periodic formation of large-scale structures in the jet shear layers using a high-spatial-resolution schlieren imaging. The entire feedback mechanism was visible and included large-scale structures in the shear layers propagating downstream and acoustic waves propagating upstream. Mitchell et al. [13] also studied the periodic oscillation of the shear layers of underexpanded impinging jets using time-resolved schlieren image sequences. Finally, Uzun et al. [14] studied the organization of the coherent structures responsible for the feedback mechanism in a nearly ideally expanded round impinging jet computed by large-eddy simulation (LES).

Unfortunately, the connections between the different flow features, namely the shock oscillations, the shear-layer instabilities, the recirculation zones near the plate, and the production of tones in nonideally expanded jets, remain unclear. Kuo and Dowling [15], however, considered that there is a feedback mechanism in the region of impact between the Mach disk and the flat plate. They developed a one-dimensional model of the Mach disk motion involving acoustic and entropy waves. A resonance condition providing, for a given velocity flow, the frequency of resonance of the Mach disk motion was thus found. Although the model was supposed to be suitable for all plates, the predicted resonance frequencies matched the experimental tone frequencies obtained by Powell [16] only for small plates whose diameter is approximately equal to the jet nozzle diameter. Moreover, the model is only valid when there is no recirculation zone between the Mach disk and the plate. Finally, for strongly underexpanded jets impinging on a plate located in the first cell of the equivalent free jets, Henderson et al. [10] identified a specific feedback loop involving turbulent structures propagating downstream in the shear layer between the subsonic region downstream of the Mach disk and the supersonic peripheral flow. A model of this feedback loop was proposed by Dauptain et al. [17,18] to predict the tone frequencies generated by the jets.

In the present work, four LESs of an underexpanded round jet impinging on a flat plate normally are carried out to investigate flow

*Ph.D. Student, Laboratoire de Mécanique des Fluides et d'Acoustique, UMR CNRS 5509; currently Postdoctoral Researcher, KTH Mechanics, Stockholm, Sweden; gojon@kth.se.

†Research Scientist, Laboratoire de Mécanique des Fluides et d'Acoustique, UMR CNRS 5509; Christophe.bogey@ec-lyon.fr. Senior Member AIAA.

structure oscillations and tone production. The jet is characterized by a nozzle pressure ratio of 4.03, an exit Mach number of 1, a fully expanded Mach number of 1.56, and a Reynolds number of 6×10^4. The location of the flat plate with respect to the jet exit section varies to study the effects of the nozzle-to-plate distance on the feedback loop. The jet flowfield and acoustic near field are described and compared with experimental data and with results of theoretical models. The presence of a Mach disk just upstream from the plate and its influence on tone generation are discussed. When such a Mach disk is formed, its oscillating behavior is analyzed. The possible links between the oscillating motion of this Mach disk and the spatial and temporal properties of the feedback mechanism are sought.

The paper is organized as follows. The jet parameters and the numerical methods used for the LES are given in Sec. II. Aerodynamic and acoustic results are given in Sec. III. In particular, the feedback mechanism establishing between the nozzle and the flat plate is investigated by evaluating the convection velocity in the jet shear layers and by describing the jet near pressure fields. An analysis of the tone generation is then conducted by studying the motions of the possible Mach disk upstream from the plate and the intermittency of the tone intensities. Concluding remarks are given in Sec. IV.

II. Parameters

A. Jet Parameters

Four large-eddy simulations of a supersonic impinging jet have been conducted, as reported in Table 1. In the four cases, the nozzle-to-plate distances L are respectively equal to $2.08D$, $2.80D$, $3.65D$, and $4.66D$, where D is the nozzle exit diameter. The simulations are thus referred to as JetL2.1, JetL2.8, JetL3.6, and JetL4.7. The jet originates from a pipe nozzle, whose lip is $0.05D$ thick, with a nozzle pressure ratio of $NPR = P_r/P_{amb} = 4.03$ and a temperature ratio $TR = T_r/T_{amb} = 1$, where P_r and T_r are the stagnation pressure and temperature, and P_{amb} and T_{amb} are the ambient pressure and temperature. At the nozzle exit, the jet has a Mach number of $\mathcal{M}_e = u_e/c_e = 1$ and an ideally expanded Mach number of $\mathcal{M}_j = u_j/c_j = 1.56$, where u_e and c_e are the velocity and speed of sound in the jet, and u_j and c_j are the velocity and speed of sound in the ideally expanded equivalent jet. Its Reynolds number is equal to $Re_j = u_j D_j/\nu = 6 \times 10^4$, where D_j is the nozzle diameter of the ideally expanded equivalent jet, and ν is the kinematic molecular viscosity. At the nozzle inlet, a Blasius boundary-layer profile of thickness $0.075D$ and a Crocco–Busemann profile are imposed for velocity and density. The ejection conditions of the jet and the ratios of the nozzle lip thickness and of the nozzle-to-plate distances with respect to the exit diameter in the simulations are identical to those in the experiments of Henderson et al. [10]. In particular, the four nozzle-to-plate distances considered in the LES are chosen because of the large amount of measurements available, including mean velocity and acoustic data, and because of their regular spacings.

To generate velocity fluctuations at the nozzle exit, low-amplitude random vortical disturbances, not correlated in the azimuthal direction, are added in the boundary layer in the nozzle, at $z = -D/4$, using a procedure detailed in a previous study [19]. The strength of the forcing allows us to obtain peak turbulent intensities of 7.7, 5.8, 5.2, and 5.1 of the fully expanded jet velocity at the nozzle exit for JetL2.1, JetL2.8, JetL3.6, and JetL4.7, respectively. The jets are thus initially highly disturbed.

B. Numerical Parameters

The unsteady compressible Navier–Stokes equations are solved in a cylindrical coordinate system (r, θ, z) by using an explicit six-stage Runge–Kutta algorithm for time integration and low-dissipation explicit 11-point centered finite differences for spatial derivation [20,21]. At the end of each time step, a six-order, 11-point filtering [22] is applied to the flow variables to remove grid-to-grid oscillations and to relax turbulent energy from scales at wave numbers close to the grid cutoff wave number. Thus, the filtering acts as a subgrid-scale model in the LES [23–26]. The radiation conditions of Tam and Dong [27] are implemented at the inflow and lateral boundaries of the computational domain. A sponge zone combining grid stretching and Laplacian filtering is also employed to damp the turbulent fluctuations before they reach the lateral boundaries. The axis singularity is treated with the method proposed by Mohseni and Colonius [28]. Notably, the first point close to the axis is located at $r = \Delta r/2$, where Δr is the radial mesh size near the axis. A reduction of the effective resolution near the origin of the polar coordinates is also implemented [29] to increase the time step of the simulation. The present numerical setup has been used in past studies to simulate round jets at a Mach number $\mathcal{M}_e = 0.9$, for instance [19,30–32]. In the present LES, adiabatic conditions are imposed at the nozzle walls and at the flat plate. A shock-capturing filtering is applied to avoid Gibbs oscillations near shocks. It consists of applying a conservative second-order filter at a magnitude determined at each time step using a shock sensor [22]. It was successfully used by de Cacqueray et al. [33] for the LES of an overexpanded jet at an equivalent Mach number of $\mathcal{M}_j = 3.3$.

The simulations are carried out using an OpenMP-based in-house solver, and a total of 180,000 iterations are computed in each case after the transient period. The simulation time is thus equal to $500D/u_j$. The cylindrical meshes contain between 171 and 217 million points, as reported in Table 2, also yielding the number of points n_r, n_θ, and n_z in the radial, azimuthal, and axial directions.

The variations of the radial and axial mesh spacings are represented in Fig. 1. The minimal axial mesh spacing is equal to $\Delta z = 0.00375D$ near the nozzle lip and the flat plate, and the maximal axial mesh spacing between the nozzle and the plate is $\Delta z = 0.0075D$ for JetL2.1 and JetL2.8 and $\Delta z = 0.015D$ for JetL3.6 and JetL4.7. The minimal radial spacing is equal to $\Delta r = 0.00375D$ at $r = D/2$, and the maximal radial spacing is $\Delta r = 0.03D$ for $2.5D \leq r \leq 7.5D$. Farther from the jet axis, a sponge zone is implemented for $r \geq 7.5D$. In the physical domain, the grids are stretched at rates lower than 1% to preserve numerical accuracy. The maximum mesh spacing of $0.03D$ allows acoustic waves with Strouhal numbers up to $St = fD_j/u_j = 5.3$ to be well propagated, where f is the frequency. Finally, it can be noted that the meshes in the near-nozzle region are similar to that used in a previous LES of an initially highly disturbed high-subsonic jet [19], for which a convergence study was conducted.

After the jet impact, wall jets develop on the flat plate. Their discretizations are discussed by considering the mesh spacings at the wall at $r = 2D$, given in Table 3 in wall units. In the four LESs, values of about $\Delta r^+ = 30$ and $(r\Delta\theta)^+ = 30$ are obtained in the wall-parallel directions, and $\Delta z^+ \simeq 5$ is found in the wall-normal direction. Given that the mesh spacings necessary to compute turbulent wall-bounded flows using LES [26,34–36] are about of $\Delta^+ = 30$ in the streamwise direction, $\Delta^+ = 1$ in the wall-normal direction, and $\Delta^+ = 10$ in the spanwise direction, the meshes appear too coarse to accurately compute the wall jets in the present

Table 1 Jet parameters

Jet	M_j	Re_j	L
JetL2.1	1.56	6×10^4	$2.08D$
JetL2.8	1.56	6×10^4	$2.80D$
JetL3.6	1.56	6×10^4	$3.65D$
JetL4.7	1.56	6×10^4	$4.66D$

Table 2 Mesh parameters

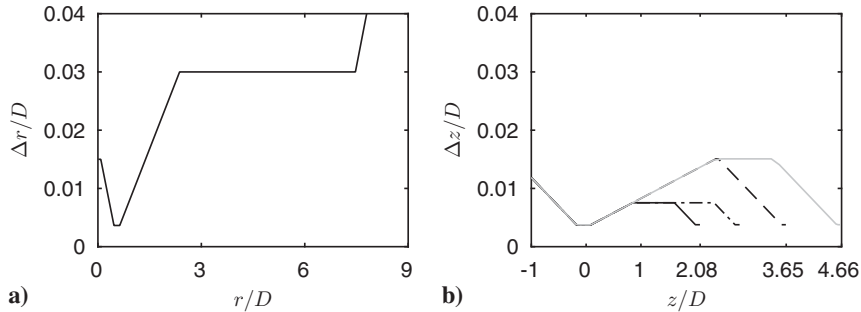| Jet	n_r	n_θ	n_z	$n_r \times n_\theta \times n_z$
JetL2.1	500	512	668	171×10^6
JetL2.8	500	512	764	195×10^6
JetL3.6	500	512	780	200×10^6
JetL4.7	500	512	847	217×10^6

Fig. 1 Representation of a) radial, and b) axial mesh spacings for JetL2.1 (black solid line), JetL2.8 (dash-dotted line), JetL3.6 (dashed line), and JetL4.7 (gray solid line).

simulations. The wall jets can, however, be expected not to affect the feedback loop and not to contribute to the acoustic field significantly due to their low velocities rapidly decreasing with the radial distance. At $r = 2D$, for instance, the peak wall jet velocities are only about $350 \text{ m} \cdot \text{s}^{-1}$; see also in Table 3.

III. Results

In this section, the results of the present LES are presented. Some numerical results obtained in Gojon et al. [37] for the jet without flat plate are also shown. The mean density field of that free jet is represented in Fig. 2, in which the positions of the plate in the impinging cases are indicated. For JetL2.1, with $L = 2.08D$, the plate is located in the first half of the second cell of the shock-cell structure, where the velocity increases and the pressure decreases with the axial distance on the jet centerline. For JetL2.8, with $L = 2.8D$, it lies in the second half of the second cell, where velocity decreases and pressure increases. Finally, for JetL3.6 and JetL4.7, with $L = 3.65D$ and $L = 4.66D$, the flat plates fall in the first halves of the third and of the fourth shock cells, respectively. These remarks are important because the production of intense tones in imperfectly expanded impinging jets appears to depend on the location of the plate in the shock-cell structure of the corresponding free jet. In the experiments of Henderson et al. [10], in particular, no tone seems to be generated when there is a whole number of shock cells between the jet nozzle and the flat plate. In that case, moreover, there is no Mach disk forming upstream from the plate.

A. Flow Snapshots

Isosurfaces of density obtained for JetL4.7 are displayed in Fig. 3. The mixing layer and the wall jet developing after the jet impingement in the radial direction are well visible. A shock-cell structure can also be seen in the jet between the nozzle and the plate. In addition, longitudinal structures appear on the outer boundary of the first shock cell. Such structures have been described in different experiments, including those by Arnette et al. [38]. They are due to the small perturbations at the nozzle exit, which are amplified by Taylor–Goertler-type instabilities. The pressure field obtained in the planes $\theta = 0$ and $\theta = \pi$ are also represented in the figure. Acoustic waves coming from the region of jet impact are observed.

Snapshots of the vorticity norm obtained in the (z, r) plane for the four impinging jets are represented in Fig. 4. For JetL2.1, in Fig. 4a, coherent vortices of typical size $0.1D$ are found in the shear layers. Downstream of a Mach disk located at $z \simeq D$, whose presence and

motions will be later discussed, two slip lines are visible, separated by a distance of about $0.25D$. For comparison, in the corresponding free jet [37], the distance between the slip lines is smaller and equal to $0.11D$ due to a Mach disk of a smaller diameter. For JetL2.8, JetL3.6, and JetL4.7, the jet shear layers exhibit both coherent and fine-scale structures. In these cases, the distance between the slip lines downstream of the Mach disk in the first shock cell is close to that in the free jet.

Snapshots of density and pressure fluctuations obtained in the (z, r) plane are provided in Fig. 5 and in a supplemental video. For JetL2.1, in Fig. 5a, one shock cell ended by a Mach disk located around $z = 0.9D$ is seen in the jet. This shock cell is shorter than the first shock cell in the corresponding free jet; see in Fig. 2. Moreover, an annular oblique shock is visible around the Mach disk, as in the free jet. In the video, the Mach disk shows a strong axial motion, as is the case in the experiments of Risborg and Soria [11] for a round underexpanded impinging jet. Moreover, sound waves propagating from the region of jet impact appear in the pressure field. For JetL2.8, in Fig. 5b, the first shock cell in the jet is similar to that in the free jet. A Mach disk forms upstream from the plate in the second shock cell at $z \simeq 2.1D$. Pressure waves seem also to be generated by the jet impact. For JetL3.6, in Fig. 5c, the two first shock cells in the jet resemble those in the free jet. In the pressure field, in addition to the sound waves coming from the region of jet impact, circular wave fronts centered around the annular oblique shock of the first cell are visible. They are most probably due to the interactions between the oblique shock and the shear-layer turbulence. Finally, for JetL4.7, in Fig. 5d, a Mach disk is found upstream from the plate at $z \simeq 3.85D$, in the third shock cell of the jet. The pressure field looks like that of JetL3.6.

B. Mean Flows

The mean velocity fields obtained in the (r, z) plane are represented in Fig. 6. As mentioned previously, the first shock cell in JetL2.1 is smaller than those in the other jets. In JetL2.8 and JetL4.7, a second cell and a third cell, respectively, cannot fully form before the plate, leading to the formation of a Mach disk close to the wall. On the contrary, in JetL3.6, the two first shock cells appear to spread over the entire space between the nozzle and the plate, and no Mach disk is created upstream from the plate. In the figure, the measurements of Henderson et al. [10] are also displayed for JetL2.1, JetL2.8, and JetL3.6. Overall, they are comparable with the simulation results. In the experiments, however, the shock cells are slightly longer, and for JetL3.6, unlike the computation, there seems to be a Mach disk just upstream from the plate.

The centerline mean axial velocity profiles obtained in the LES and in the experiments of Henderson et al. [10] are displayed in Fig. 7. The profiles provided by the LES of Dauptain et al. [17,18] for the nozzle-to-plate distances of $L = 2.08D$ and $L = 4.16D$ are also plotted in Figs. 7a and 7d, respectively. It can first be noted that, in all cases, the velocity in the first half of the first shock cell is slightly higher in the simulations than in the experiment. Despite this, for JetL2.1, the present results are in good agreement with both experimental and numerical data. The LES profile indicates the presence of a Mach disk at $z_p = 0.97D$, as reported in Table 4. For

Table 3   Mesh spacings on the plate and maximal mean velocity at $r = 2D$

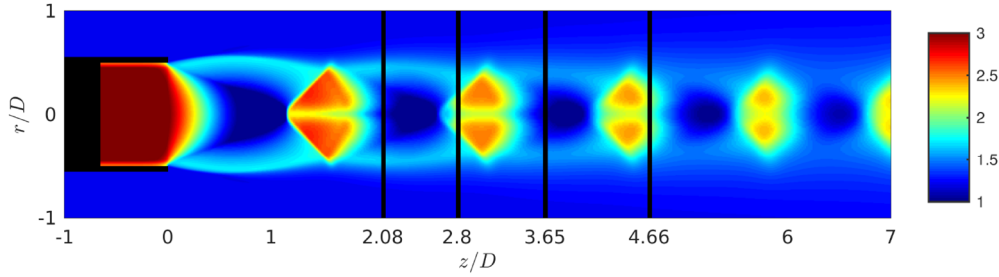| Jet	Δz^+	Δr^+	$(r\Delta\theta)^+$	Wall jet velocity, $\text{m} \cdot \text{s}^{-1}$
JetL2.1	4.5	24	31	305
JetL2.8	5.3	28	35	365
JetL3.6	5.4	29	36	375
JetL4.7	5.4	28	35	360

Fig. 2 Mean density field obtained for the jet without flat plate, using a color scale from 1 to 3 kg · m⁻³; positions of the flat plate in the impinging cases (solid lines).

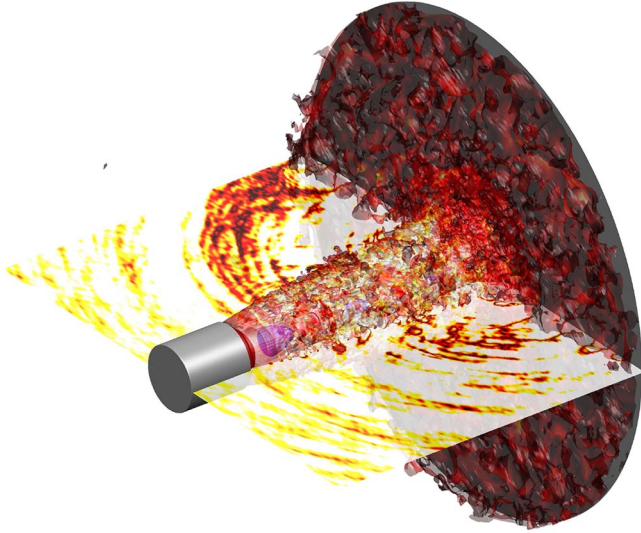**Fig. 3** Isosurfaces of density for JetL4.7: in blue and red for the values of 0.8 and 2.5 kg · m⁻³, colored by the local Mach number for 1.25 kg · m⁻³; and pressure at $\theta = 0$ and π.

JetL2.8, the LES and experimental results are roughly similar but are significantly different between the Mach disk at $z = 1.1D$ and the Mach disk located upstream from the plate at $z_p = 2.12D$. These differences are most likely due to the particle lag occurring behind the Mach disk when performing the particle image velocimetry measurements in the experiments [10]. For JetL3.6, as noted previously, no Mach disk appears to form just upstream from the flat plate, contrary to the experiment. This discrepancy may be due to the slight differences in the shock-cell structure visible in Fig. 6c, which likely result from the use of a pipe nozzle in the LES and a converging nozzle in the experiment. Finally, for JetL4.7, the present results compare favorably with the experimental data, both showing the presence of a Mach disk at $z_p = 3.86D$. In the region between $z = 0$ and $z \simeq 3D$, where the two first shock cells are found, they are also very close to the LES results obtained by Dauptain et al. [17,18] for the nozzle-to-plate distance of $L = 4.16D$, confirming the hypothesis of a particle lag occurring behind the Mach disk in the experiment.

Figure 7 moreover suggests the presence of a recirculation zone near the plate in all cases, in agreement with the experiments of Henderson and Powell [8], Krothapalli et al. [9], and Henderson et al. [10]. For JetL2.1, JetL2.8, and JetL4.7, in which there is a Mach disk near the plate, this result is consistent with the observations of Kuo and Dowling [15], who noted the appearance of a recirculation zone when the distance between the Mach disk and the plate exceeds $0.6D$. For JetL2.1, JetL2.8, and JetL4.7, indeed, this distance, given in Table 4, is equal to $1.11D$, $0.68D$, and $0.8D$, respectively.

For completeness, the mean axial velocity profiles obtained at $z = 0.75D$, $z = 1.5D$, and $z = 1.8D$ for JetL2.1 are represented in Fig. 8. They are found to be in good agreement with the measurements of Henderson et al. [10] and the numerical results of Dauptain et al. [17,18].

C. Convection Velocity

The convection velocity of the jet flow structures are estimated from axial velocity cross-correlations along the path where the turbulence intensity is maximal; see in Fig. 9 for JetL4.7, for instance.

The results thus obtained are shown in Fig. 10a. In the four impinging jets, they are very similar and appear to vary according to the shock-cell structure. In the first shock cell, the convection velocity increases between the nozzle and the Mach disk, as the jet velocity grows, and then decreases following the reduction in jet velocity. The peak is reached around $z = 0.95D$ for JetL2.1 and $z = 1.15D$ for the other jets, due to the shorter shock cell in the first case. Similar oscillations of the convection velocity are noted in the other shock cells. They are consistent with the experimental results obtained by André [39] for imperfectly expanded round jets. For comparison, the convection velocity evaluated in the corresponding free jet [37] is also plotted in the figure. Far downstream from the jet exit, values of about $0.65u_j$ are obtained, which is in good agreement with the experiments of Harper-Bourne and Fisher [40], who measured $u_c = 0.70u_j$ using a crossed-beam schlieren technique.

The mean convection velocities between the jet nozzle and the flat plate in the present LES are displayed in Fig. 10b as a function of the nozzle-to-plate distance L. They increase from $0.54u_j$ for JetL2.1 up to $0.59u_j$ for JetL4.7. As shown in the figure, they appear to be well predicted by the expression

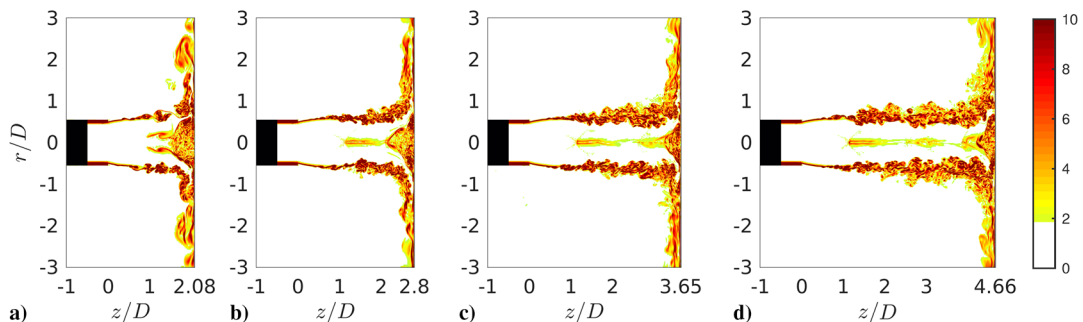$$\langle u_c \rangle(L) = 0.65u_j - (0.65u_j - 0.5u_e)\frac{1}{1 + L/D_j} \tag{1}$$

Fig. 4 Snapshots of the vorticity norm for a) JetL2.1, b) JetL2.8, c) JetL3.6, and d) JetL4.7. The color scale ranges up to the level of $10u_e/D$.
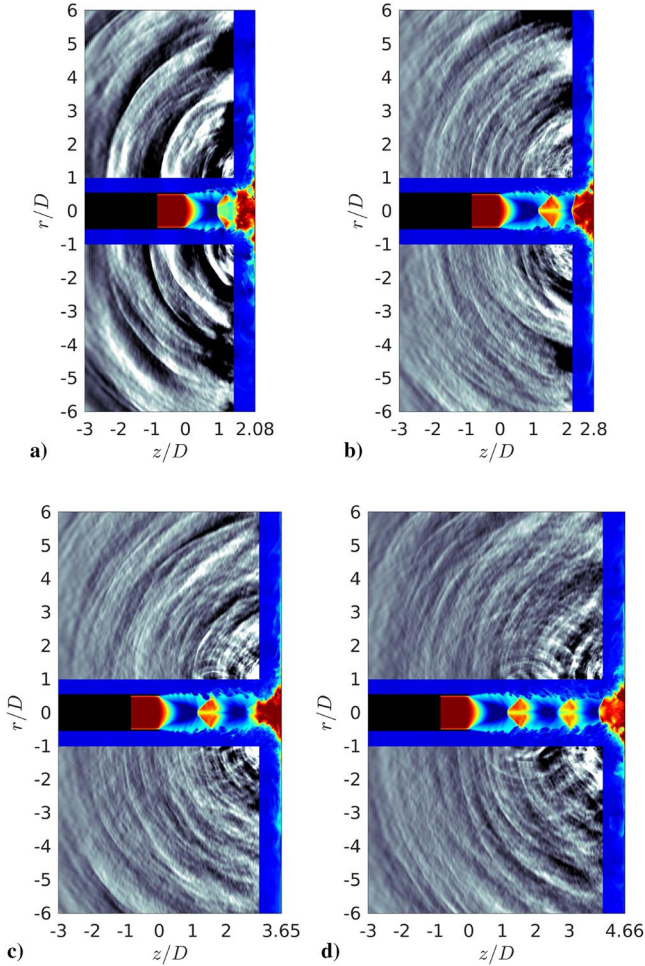
Fig. 5 Snapshots of density in the jet and near the flat plate and of pressure fluctuations for a) JetL2.1, b) JetL2.8, c) JetL3.6, and d) JetL4.7. The color scales range from 1 to 3 kg · m⁻³, and from −2000 to 2000 Pa.

which, moreover, tends to $0.65u_j$ for large distances L and to $0.5u_e$ for small distances L, as expected for instabilities initially growing in the mixing layers just downstream of the nozzle.

D. Pressure Spectra

The pressure spectra obtained close to the nozzle at $r = D$ and $z = 0$ are plotted in Fig. 11 as a function of the Strouhal number $St = fD_j/u_j$. The Strouhal numbers of the tones whose levels are 5 dB higher than the broadband noise are given in Table 5.

For JetL2.1, in Fig. 11a, three tones are found at Strouhal numbers $St_1 = 0.375$, $St_2 = 0.505$, and $St_3 = 1.01$, with $St_3 = 2St_2$. The dominant tone, which is 20 dB above the broadband noise, is at St_2. This result agrees with the experiments of Henderson et al. [10], who obtained a fundamental tone at $St = 0.52$. For JetL2.8, in Fig. 11b, several tones are observed between $St = 0.3$ and $St = 2$, with two

main tones visible at $St_1 = 0.335$ and $St_2 = 0.415$. The latter value corresponds to the dominant tone frequency and is very close to the fundamental tone frequency at $St = 0.41$ of the experiments [10]. For JetL3.6, in Fig. 11c, two tones are around 6 dB above the broadband noise. The dominant tone frequency at $St_1 = 0.345$ compares well with the fundamental tone frequency at $St = 0.32$ acquired experimentally [10]. Given the presence in the jet of a Mach disk just upstream from the plate in the experiment and its absence in the LES, the main frequency of the feedback mechanism therefore appears not to depend on the formation of such a structure. This result suggests that the feedback path lies outside the jet, in the shear layers. Finally, for JetL4.7, in Fig. 11d, the fundamental tone is at the Strouhal number of $St_2 = 0.34$.

The tones emerging in the LES pressure spectra are stronger for JetL2.1, JetL2.8, and JetL4.7 than for JetL3.6, which is the only case for which no Mach disk is found close to the flat plate. Thus, the intensity of the feedback loop seems to be affected by the presence of a near-wall Mach disk. This trend is consistent with the experiments of Henderson and Powell [8], who noted that the feedback mechanism in impinging jets establishes when there is a Mach disk upstream from the plate but ceases when there is a conical shock wave.

Moreover, it is worth reporting that, for the jet [37] without flat plate, two screech tones emerge in the pressure spectrum at $r = D$ and $z = 0$ at the Strouhal numbers of $St = 0.28$ and $St = 0.305$. These two tones are not observed for the impinging jets. Therefore, the presence of the flat plate in the second, third, or fourth shock cell of the jet appears to lead to their suppression.

E. Tone Frequencies

The feedback mechanism in supersonic impinging jets suggested by Powell [1] consists of two steps. First, in the jet shear layers, a coherent structure is convected downstream from the nozzle to the flat plate. It impinges on the plate and then generates an acoustic wave propagating upstream. This wave is reflected back by the nozzle lips, which excites the shear layer, and leads to the formation of a new coherent structure. The fundamental period T_0 of this feedback loop is given by the sum of the time necessary for a shear-layer structure to travel from the nozzle down to the plate and the time of propagation of an acoustic wave from the plate up to the nozzle, yielding

$$T_0 = \int_0^L \frac{dz}{u_c(z)} + \frac{L}{c_0} = \frac{N + p}{f} \qquad (2)$$

where $u_c(z)$ is the convection velocity in the mixing layers; c_0 is the speed of sound in the ambient medium; p is a phase lag at the nozzle exit; and the mode number N indicates the number of times the feedback mechanism occurs during the period T_0. According to Powell [1], the phase lag p is not necessarily zero because the reflection of the acoustic wave on the nozzle lips and the creation of a coherent structure in the shear layers do not happen simultaneously. For instance, values of $p = 0$ and $p = -0.4$ were respectively found for subsonic and supersonic round jets in the experiments of Krothapalli et al. [9]. Nevertheless, by setting $p = 0$, the following model was proposed by Ho and Nosseir [5]
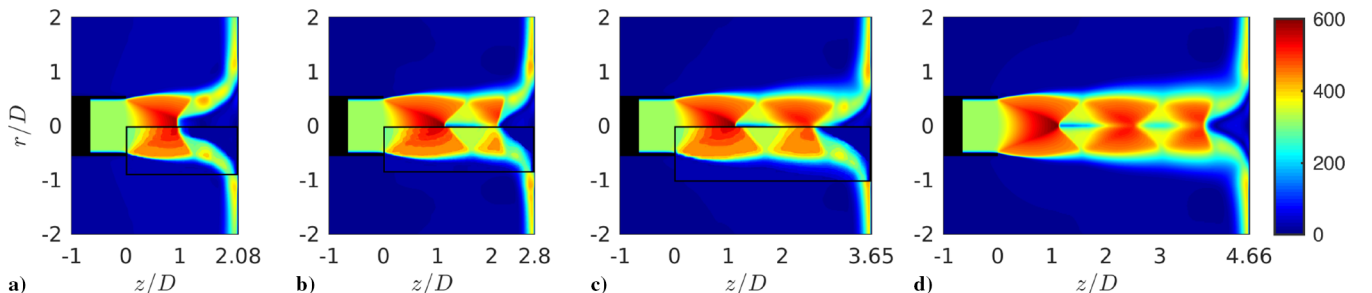

Fig. 6 Mean velocity fields for a) JetL2.1, b) JetL2.8, c) JetL3.6, and d) JetL4.7. The color scale ranges from 0 to 600 m · s⁻³. The measurements of Henderson et al. [10] are represented in the rectangles.
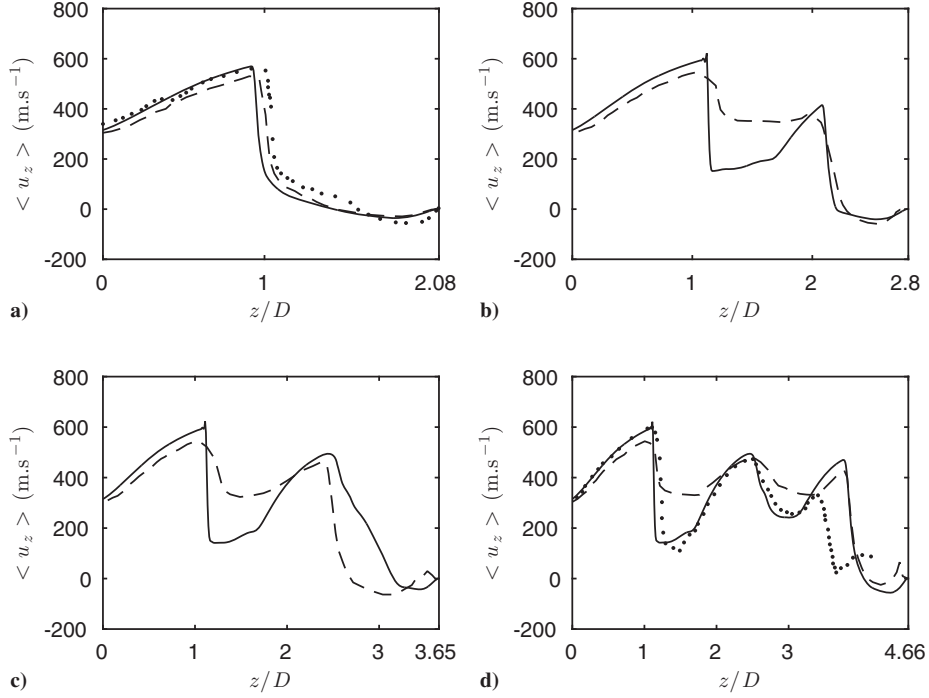
Fig. 7 Centerline profiles of mean axial velocity for a) JetL2.1, b) JetL2.8, c) JetL3.6, and d) JetL4.7: present results (solid line), Henderson et al. [10] (dashed line), and Dauptain et al. [17,18] (circles).

and Nosseir and Ho [6] to predict the frequencies of the feedback mechanism in jets impinging on a flat plate normally:

$$\frac{N}{f} = \frac{L}{\langle u_c \rangle} + \frac{L}{c_0} \qquad (3)$$

where $\langle u_c \rangle$ is the mean convection velocity in the shear layers between the nozzle and the plate.

The Strouhal numbers of the dominant tones in the present jets, reported in Table 5, are represented in Fig. 12 as a function of the nozzle-to-plate distance. The tone frequencies obtained in the experiments of Henderson et al. [10,41] for underexpanded impinging round jets with NPR = 3.80, 4.03, 4.15, and 4.50, and frequencies predicted by Eq. (3), are also displayed. In the latter case, the mean convection velocity $\langle u_c \rangle$ is provided by expression (1).

The tone Strouhal numbers in the LES are comparable with the experimental results. They also seem to be roughly predicted by model Eq. (3). The differences obtained in this case may be partially due to the approximation of the mean convection velocity by expression (1). The main tones in the LES can be associated with the second and third modes of the model for JetL2.1 and JetL2.8, with the third and fourth modes for JetL3.6, and with the third, fourth, and fifth modes for JetL4.7. Moreover, as the nozzle-to-plate distance increases, the dominant tone frequency of the feedback loop, given in Table 5, switches from the third mode to the fourth mode. It thus remains between $St = 0.34$ and $St = 0.505$ in the present jets. Such a staging behavior of the dominant tone frequency is typical of feedback mechanisms; see the experiments of Wagner [2] and Henderson [41], for instance.

Table 4 Position of the Mach disk upstream from the plate

Jet	z_p	$L - z_p$
JetL2.1	0.97D	1.11D
JetL2.8	2.12D	0.68D
JetL3.6	— —	— —
JetL4.7	3.86D	0.8D

F. Fourier Decomposition of the Pressure Field

To determine the amplitude and phase fields associated with the dominant tones of the feedback loop in the present jets, a Fourier transform in time is applied to the near pressure fields recorded every 50th LES time step in the (z, r) plane. The results obtained for the two main tones frequencies of JetL2.1 are represented in Fig. 13. For $St_1 = 0.375$, the Mach disk and the annular oblique shock are visible in the jet in the amplitude field of Fig. 13a. A 180 deg phase shift with respect to the jet axis is found in the phase field of Fig. 13b, indicating a sinuous or helical oscillation mode. More precisely, the mode is helical, as illustrated by the azimuthal distributions of the pressure filtered around St_1 at three times separated by $T_1/3$, where T_1 is the period associated with St_1, shown in Fig. 14a. For that jet, and for the three others, a more in-depth investigation of the azimuthal organizations of the acoustic waves in the nozzle-exit plane and of the turbulent structures on the flat plate at the tone frequencies can be found in a recent paper [42].

For $St_2 = 0.505$, in the amplitude field of Fig. 13c, two lobes appear just outside of the shear layers, and two semilobes can also be seen near the nozzle and near the flat plate. By considering the two semilobes as one lobe, there are three lobes between the nozzle and the plate. The phase in Fig. 13d is identical on both sides of the jet axis, suggesting that the corresponding oscillation mode may be axisymmetrical. The latter claim is confirmed by Fig. 14b yielding azimuthal distributions of the pressure filtered around St_2 at three times separated by $T_2/4$, where T_2 is the period associated with St_2. An axisymmetrical jet oscillation was also obtained in the experiments of Henderson et al. [10]. Moreover, for St_2, two acoustic components appear in the amplitude field. The first component can be seen on both sides of the jet for $\alpha \leq 20$ deg, where α is the angle between the upstream direction and the propagation direction from the impingement region as illustrated in Fig. 13a. This component is related to the acoustic waves that close the feedback mechanism. The second component is visible for $40 \leq \alpha \leq 70$ deg. It seems to be generated near the plate at $r \simeq 1.5D$, where intense levels are found in the amplitude field. A similar observation was made in the corresponding experiments of Henderson et al. [10], which revealed acoustic sources at $r = 1.3D$ on the flat plate.

The amplitude and phase fields obtained for JetL2.8 at the two main tone Strouhal numbers $St_1 = 0.335$ and $St_2 = 0.415$ are
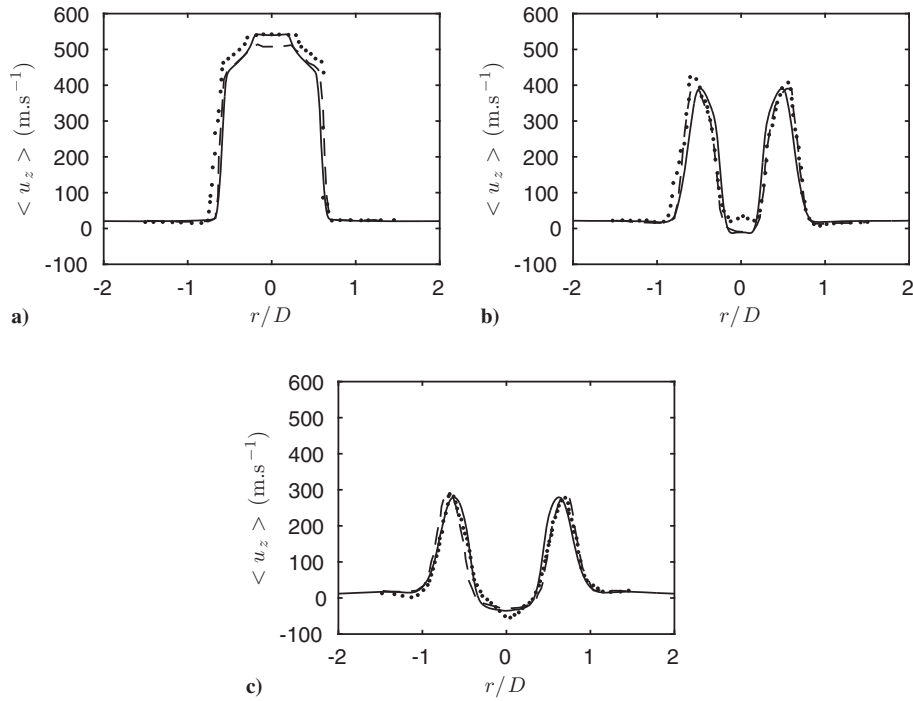
Fig. 8 Radial profiles of mean axial velocity at a) $z = 0.75D$, b) $z = 1.5D$, and c) $z = 1.8D$ for JetL2.1: present results (solid line), Henderson et al. [10] (dashed line), and Dauptain et al. [17,18] (circles).
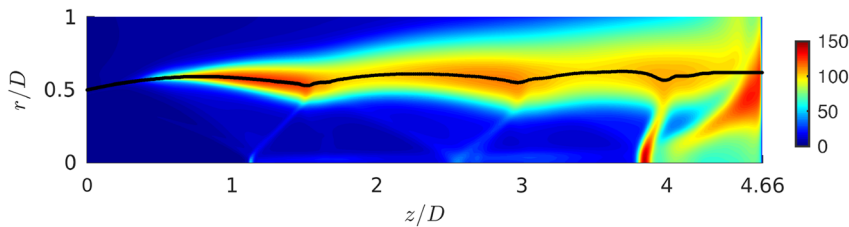

Fig. 9 Root-mean-square values of velocity fluctuations for JetL4.7. The color scale ranges from 0 to 150 m · s^{-1}. The black line shows the position of the peaks.
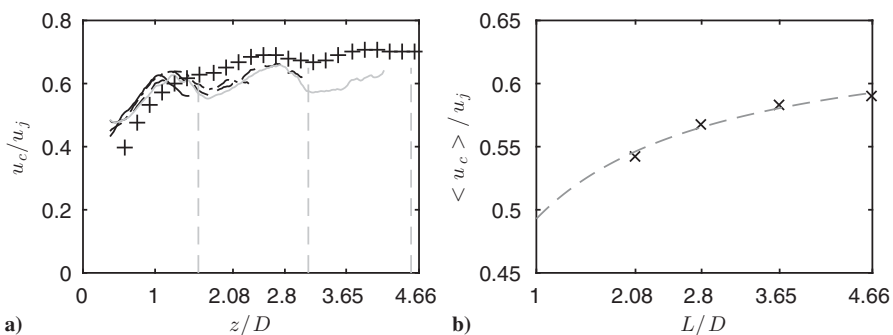

Fig. 10 Representations of a) convection velocity for JetL2.1 (solid line), JetL2.8 (dash-dotted line), JetL3.6 (dashed line), JetL4.7 (solid gray line), the free jet (+), and shock cells in that jet (vertical line); b) mean convection velocity from LES (×) and expression (1) (dashed line).

represented in Fig. 15. Two and three lobes are found between the nozzle and the plate in the amplitude fields of Figs. 15a and 15c, respectively. The phase fields of Figs. 15b and 15d as well as azimuthal distributions of pressure similar to those of Fig. 14a, not shown here for brevity, also indicate that both tones are associated with helical oscillation modes. Moreover, for the dominant tone at St_2, two acoustic components can be observed in Fig. 15c, as was the case for JetL2.1 in Fig. 13c. The second component here seems to come from a point located on the plate at $r \simeq 2D$.

The amplitude and phase fields obtained for JetL3.6 at the two main tone Strouhal numbers $St_1 = 0.345$ and $St_2 = 0.42$ are given in

Fig. 16. Three and four lobes appear between the nozzle and the plate in the amplitude fields of Figs. 16a and 16c, respectively. Furthermore, as before for JetL2.8, both tones are associated with helical oscillation modes; see the phase fields of Figs. 16b and 16d.

The results obtained for JetL4.7 at three main tone Strouhal numbers $St_1 = 0.27$, $St_2 = 0.34$, and $St_3 = 0.42$ are provided in Fig. 17. Three and four lobes are visible between the nozzle and the plate in the amplitude fields of Figs. 17a and 17c, respectively. It is, however, difficult to estimate the number of lobes in the amplitude field in Fig. 17e. In addition, given the phase fields, these three tones are linked to helical oscillation modes. Finally, for the dominant tone
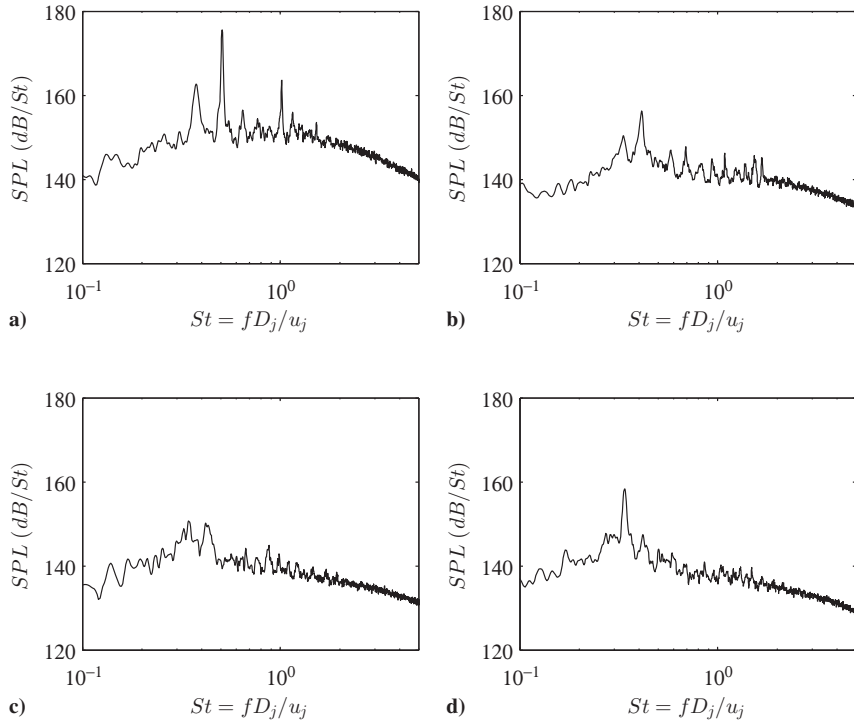
Fig. 11 Sound pressure levels at $r = D$ and $z = 0$ as a function of the Strouhal number for a) JetL2.1, b) JetL2.8, c) JetL3.6, and d) JetL4.7.

at St_2, two acoustic components are observed in Fig. 17c, as for JetL2.1 and JetL2.8. The origin of the second one seems to be a point at $r \simeq 2D$ on the plate.

For the present jets, in most cases, the amplitude fields obtained for the main tone frequencies thus exhibit lobes between the nozzle lips and the plate, whose number is equal to the mode number predicted by model Eq. (3). As discussed in a recent study for planar supersonic impinging jets [43], these lobes result from the presence of hydrodynamic–acoustic standing waves. They are found both when there is a Mach disk just upstream from the plate, as in JetL2.1, JetL2.8, and JetL4.7, and when this is not the case, as in JetL3.6.

G. Motions of the Near-Wall Mach Disk

The motions of the Mach disk close to the flat plate in JetL2.1 are illustrated in Fig. 18 showing density snapshots at four times separated by $T_2/4$, where T_2 is the time period corresponding to $St_2 = 0.505$, and in a supplemental video. An axially pulsing mode of the Mach disk near the jet axis and of the peripheral annular oblique shock is observed. The mean position of the Mach disk, $z_p = 0.97D$, is also represented. The Mach disk is located downstream of z_p in Fig. 18a, at $z = z_p$ in Fig. 18b, upstream of z_p in Fig. 18c, and again at $z = z_p$ in Fig. 18d. It thus appears to oscillate at the frequency of the dominant tone of the feedback mechanism. Moreover, a flapping motion of the annular oblique shock is noted, leading to alternating periods of compression and expansion downstream from the Mach disk.

To analyze the near-wall shock motions in JetL2.1 more quantitatively, the time variations of the positions $z - z_p$ of the shock at $r = 0$ and $r = 0.35D$ are represented in Fig. 19a. These positions are determined by tracking the maxima of the gradient of axial
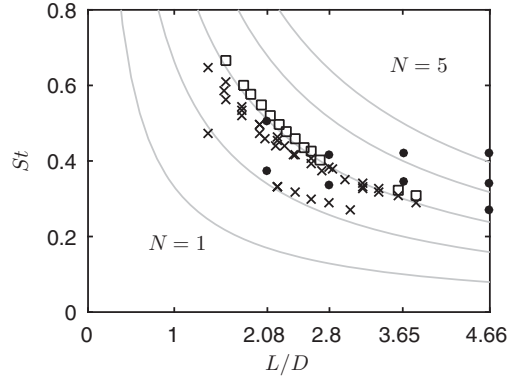

Fig. 12 Strouhal numbers of tone frequencies as a function of L/D from LES (circles), experiments [10,41] for NPR $= 4.03$ (squares) and for NPR $= 3.80, 4.15,$ and 4.50 (×), and expression (3) (solid line).

velocity. The spectra calculated from the time signals are plotted in Fig. 19b. They are normalized by the peak level reached in the two spectra. At $r = 0$, the Mach disk position oscillates around a mean position of $z_p = 0.97D$ with a standard deviation of $0.018D$. Even more, its motion is nearly periodic at the Strouhal number of $St = 0.505$, which is also the dominant tone frequency of the feedback loop. This result agrees well with the LES data of Dauptain et al. [18] for the same impinging jet and with the measurements of Risborg and Soria [11] for an underexpanded jet at a fully expanded Mach number of $\mathcal{M}_j = 1.71$ impinging on the plate two diameters downstream from the nozzle. The amplitude of the variations of the distance between the nozzle and the Mach disk was, however, equal to 11% in the latter case, whereas it is only 3.7 in the present jet.

The results obtained at $r = 0.35D$ in Fig. 19 provide information on the motion of the oblique shock surrounding the Mach disk. This shock appears to move around a mean position of $z_p = 1.13D$ with a standard deviation of $0.027D$, at a dominant Strouhal number of $St = 0.505$ as the Mach disk. Moreover, the time variations of the Mach disk and of the oblique shock positions are in phase, which is consistent with the axisymmetric nature of the jet oscillation mode at $St_2 = 0.505$. The amplitude of the oscillations of the oblique shock

Table 5   Strouhal numbers emerging in the spectra of Fig. 11

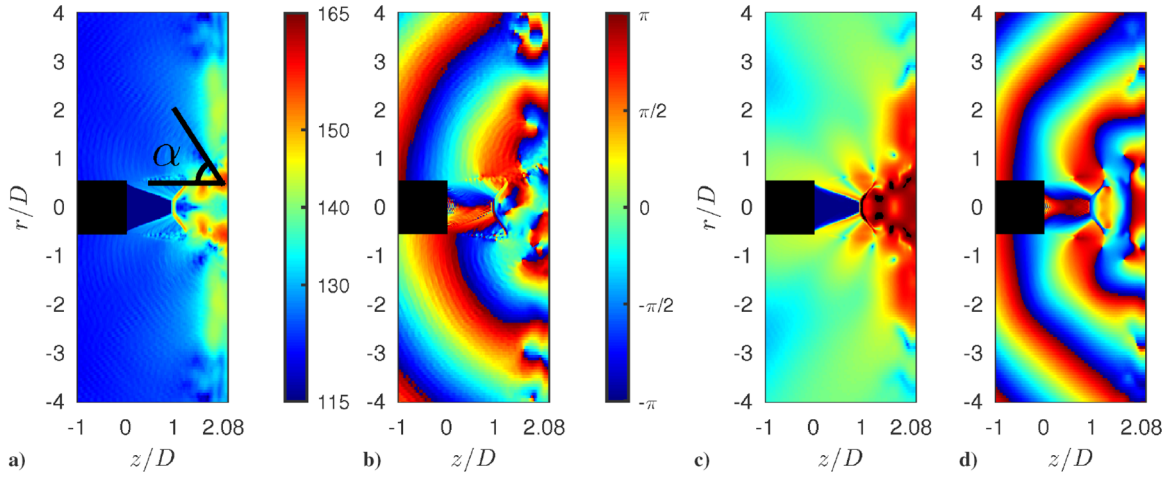| Jet	St_1	St_2	St_3
JetL2.1	0.375	0.505 (dominant)	1.01
JetL2.8	0.335	0.415 (dominant)	— —
JetL3.6	0.345 (dominant)	0.42	— —
JetL4.7	0.27	0.34 (dominant)	0.42

Fig. 13 Amplitude and phase fields obtained for JetL2.1: a–b) at $St_1 = 0.375$, and c–d) at $St_2 = 0.505$. The color scales range from 115 to 165 dB · St^{-1} for the amplitude and from $-\pi$ to π for the phase.
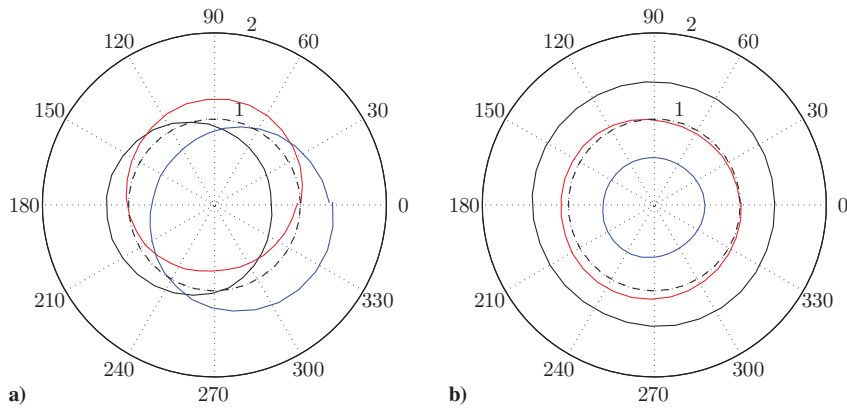

Fig. 14 Normalized azimuthal distributions of pressure for JetL2.1: a) filtered around St_1 at three times separated by $T_1/3$, and b) filtered around St_2 at three times separated by $T_2/4$; unit circle (dashed line).
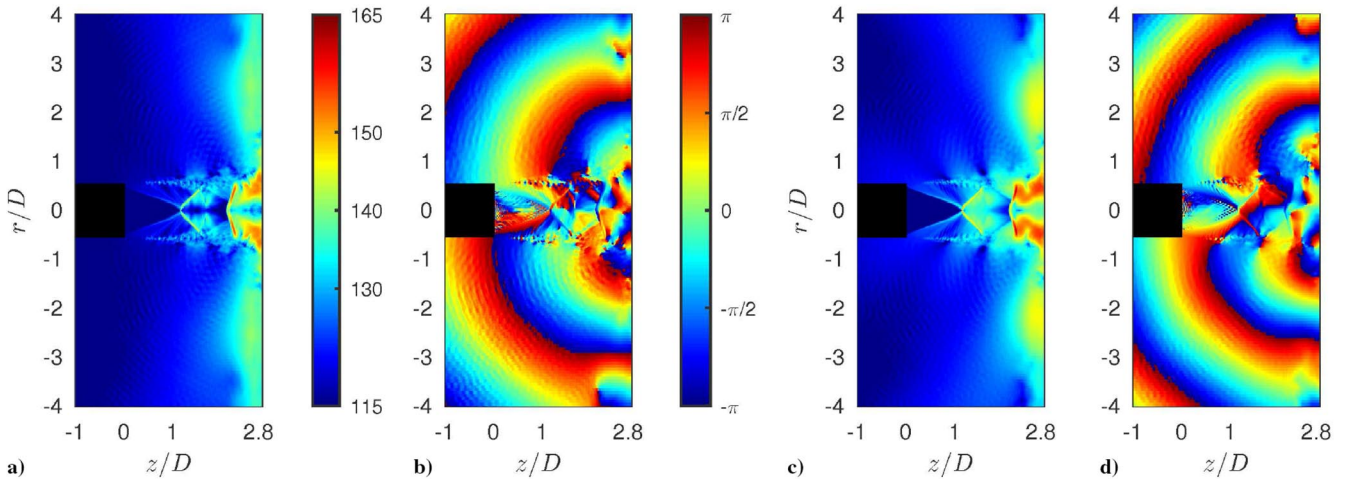

Fig. 15 Amplitude and phase fields obtained for JetL2.8: a–b) at $St_1 = 0.335$, and c–d) at $St_2 = 0.415$. The color scales range from 115 to 165 dB · St^{-1} for the amplitude and from $-\pi$ to π for the phase.

position is, however, slightly higher. Finally, it can be pointed out that, in Fig. 19b, the tone Strouhal number $St_1 = 0.375$ of the feedback loop in JetL2.1 emerges neither in the spectrum at $r = 0.35D$ nor in that at $r = 0.35D$.

In the same way as for JetL2.1, the time variations of the positions $z - z_p$ of the near-wall shock at $r = 0$ and $r = 0.35D$ and their associated spectra are provided in Fig. 20 for JetL4.7, that is for the case with the largest nozzle-to-plate spacing. A supplemental video is also provided. The shock position varies around $z_p = 3.86D$ with a

standard deviation of $0.030D$ on the jet axis and around $z_p = 3.96D$ with an amplitude of $0.037D$ at $r = 0.35D$. Thus, on average, the shock is not perfectly straight. In addition, it oscillates over a greater axial distance at $r = 0.35D$ than at $r = 0$, apparently nearly periodically in the former case but not in the latter. In Fig. 20b, the spectrum obtained for $r = 0.35D$ is indeed dominated by a tone at $St = 0.34$, which is the dominant tone frequency of the feedback loop in JetL4.7, whereas the spectrum for $r = 0$ is broadband. These results, and azimuthal distributions of the shock position at $r = 0.35D$
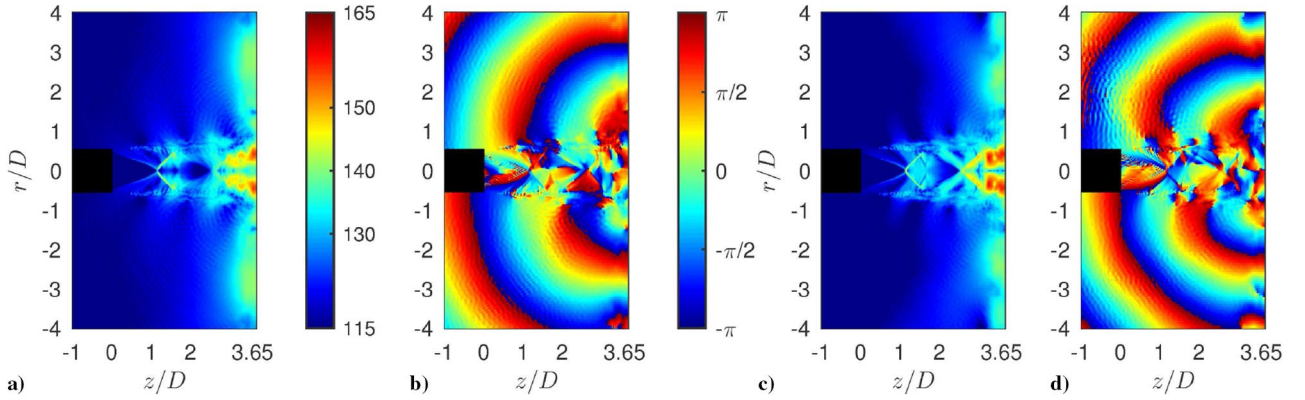
Fig. 16 Amplitude and phase fields obtained for JetL3.6: a–b) at $St_1 = 0.345$, and c–d) at $St_2 = 0.42$. The color scales range from 115 to 165 dB $\cdot$ St^{-1} for the amplitude and from $-\pi$ to π for the phase.
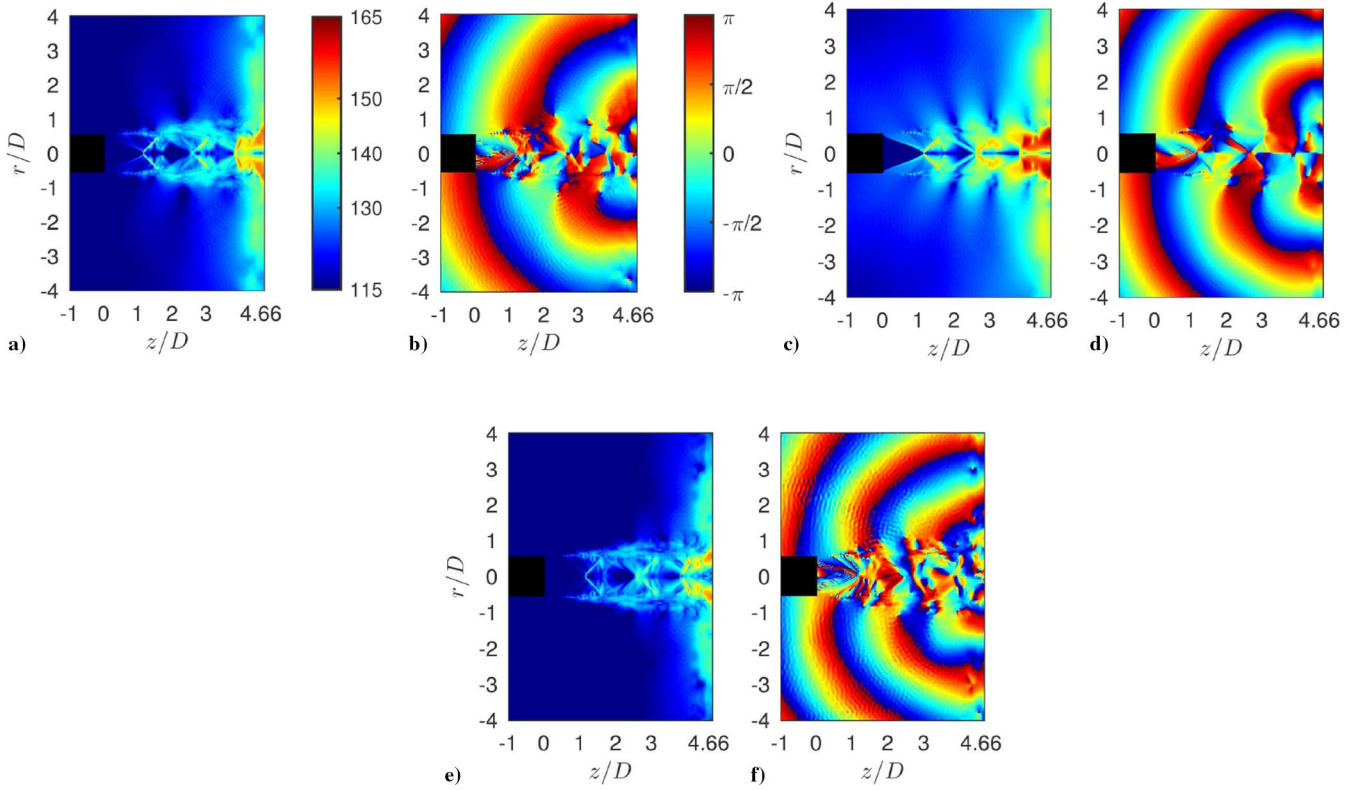

Fig. 17 Amplitude and phase fields obtained for JetL4.7: a–b) at $St_1 = 0.27$, c–d) at $St_2 = 0.34$, and e–f) at $St_3 = 0.42$. The color scales range from 115 to 165 dB $\cdot$ St^{-1} for the amplitude and from $-\pi$ to π for the phase.
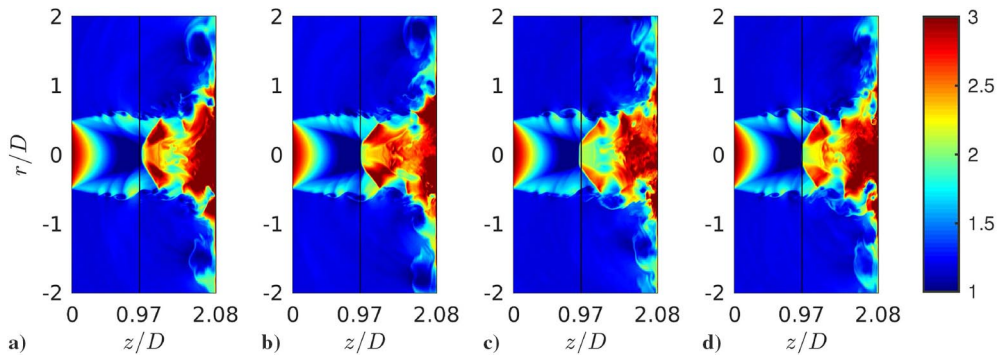

Fig. 18 Density snapshots obtained for JetL2.1 at four times separated by $T_2/4$, using a color scale ranging from 1 to 3 kg $\cdot$ m^{-3}; mean position of the Mach disk (solid line).

not shown here, indicate that the motion of the Mach disk is helical, which seems natural given the helical nature of the jet oscillation mode $St_2 = 0.34$. Note that a helical impinging mode was also observed in the experiments of Risborg and Soria [11] for an underexpanded jet at a fully expanded Mach number of $\mathcal{M}_j = 1.56$ impinging a plate located two diameters downstream from the nozzle.
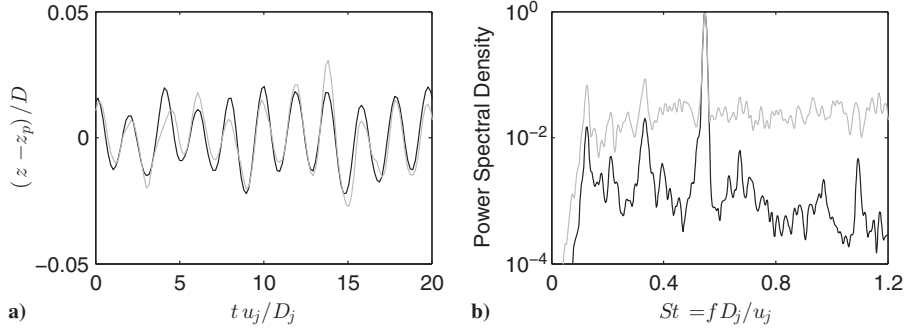
Fig. 19   Axial positions of the near-wall shock at $r = 0$ (black line) and at $r = 0.35D$ (gray line) in JetL2.1: a) time variations, and b) spectra of time variations normalized by the peak level.
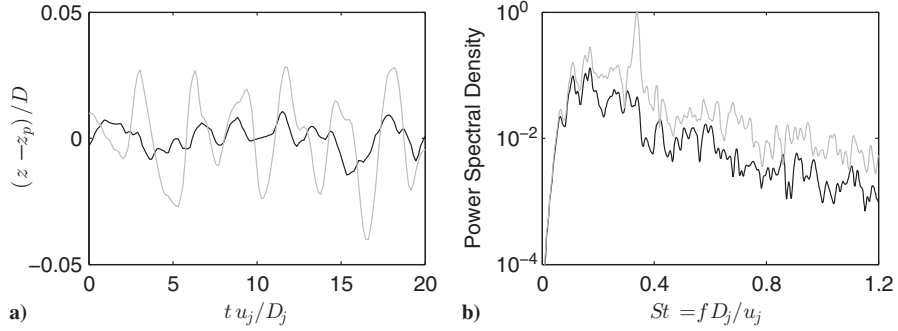

Fig. 20   Axial positions of the near-wall shock at $r = 0$ (black line) and at $r = 0.35D$ (gray line) in JetL4.7: a) time variations, and b) spectra of time variations normalized by the peak level.
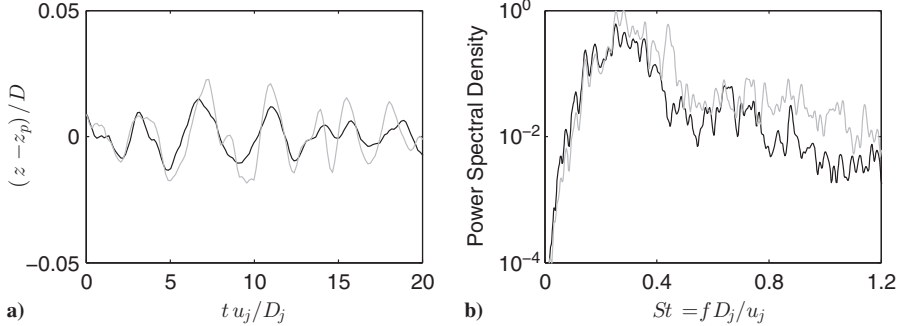

Fig. 21   Axial positions of the near-wall shock at $r = 0$ (black line) and at $r = 0.35D$ (gray line) in JetL2.8: a) time variations, and b) spectra of time variations normalized by the peak level.

Finally, the motion of the near-wall shock in JetL2.8, in which a Mach disk also forms close to the flat plate, is characterized in Fig. 21 as before for JetL2.1 and JetL4.7. The shock position oscillates around $z_p = 2.12D$ with a standard deviation of $0.012D$ on the jet axis and around $z_p = 2.21D$ with an amplitude of $0.014D$ at $r = 0.35D$. Thus, as for JetL4.7, the shock is not perfectly straight. In this case, the results obtained at $r = 0$ and $r = 0.35D$ do not differ much. In particular, the spectra of Fig. 21b are broadband, implying that the Mach disk motion is not simply periodic. A tone at $St = 0.415$, which is also the main tone frequency of the feedback loop in JetL2.8, is however visible at $r = 0.35D$ but is not at $r = 0$. Therefore, at this Strouhal number, the motion of the Mach disk is most likely helical, as is the case for the jet oscillation mode.

H.   Tone Intermittency

To determine whether the acoustic tones are produced simultaneously or alternatively in the four impinging jets, a Fourier transform is applied to the pressure fluctuations at $r = D$ and $z = 0$ using a sliding window of size $35u_j/D_j$. The spectra thus obtained are represented in Fig. 22 as functions of time and Strouhal number. For JetL2.1, the two tones of the feedback loop at $St_1 = 0.375$ and $St_2 = 0.505$ emerge in the spectrum. The intensity of the dominant tone at St_2 seems to be nearly constant, whereas that of the tone at St_1 varies in time. For JetL2.8 and JetL3.6, the levels obtained at the different tone Strouhal numbers (at $St_1 = 0.335$ and $St_2 = 0.415$ in the former case and at $St_1 = 0.345$ and $St_2 = 0.42$ in the latter) all appear to fluctuate. For JetL4.7, the magnitude of the dominant tone at $St_2 = 0.34$ does not change much, whereas those of the tones at $St_1 = 0.27$ and $St_3 = 0.42$ evolve in time.

The sound pressure levels obtained for the tone frequencies are represented in Fig. 23 as a function of time. For JetL2.1, the intensity of the tone at $St_2 = 0.505$ remains between 173 and 174 dB/St, whereas that of the tone at $St_1 = 0.375$ varies between 145 and 156 dB/St. For JetL2.8, the strong oscillations of the intensities of the tones at $St_1 = 0.335$ and $St_2 = 0.415$ appear to be 180 deg out of phase, given that the maximal values reached for St_1 coincide roughly with the minimal values for St_2 and inversely. At $t \simeq 180D_j/u_j$, for instance, values of 137 and 161 dB/St are respectively found. These results suggest a switch between the two tones. For JetL3.6, a similar
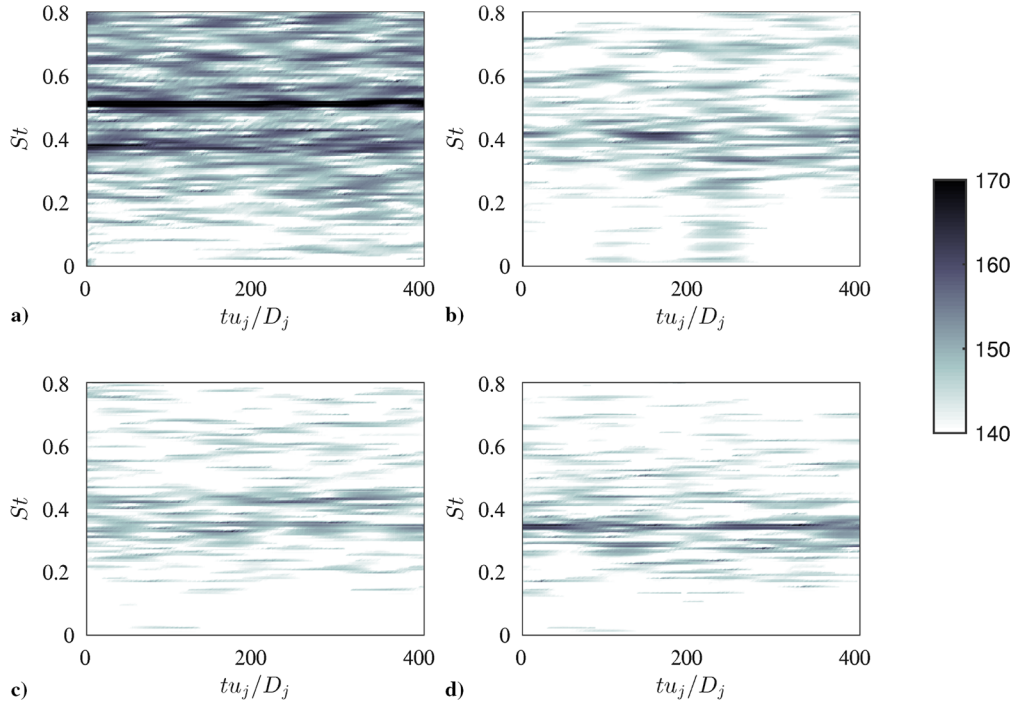
Fig. 22 Sound pressure levels obtained at $r = D$ and $z = 0$ as functions of time and Strouhal number for a) JetL2.1, b) JetL2.8, c) JetL3.6, and d) JetL4.7. The color scale ranges from 130 to 170 dB $\cdot$ St^{-1}.
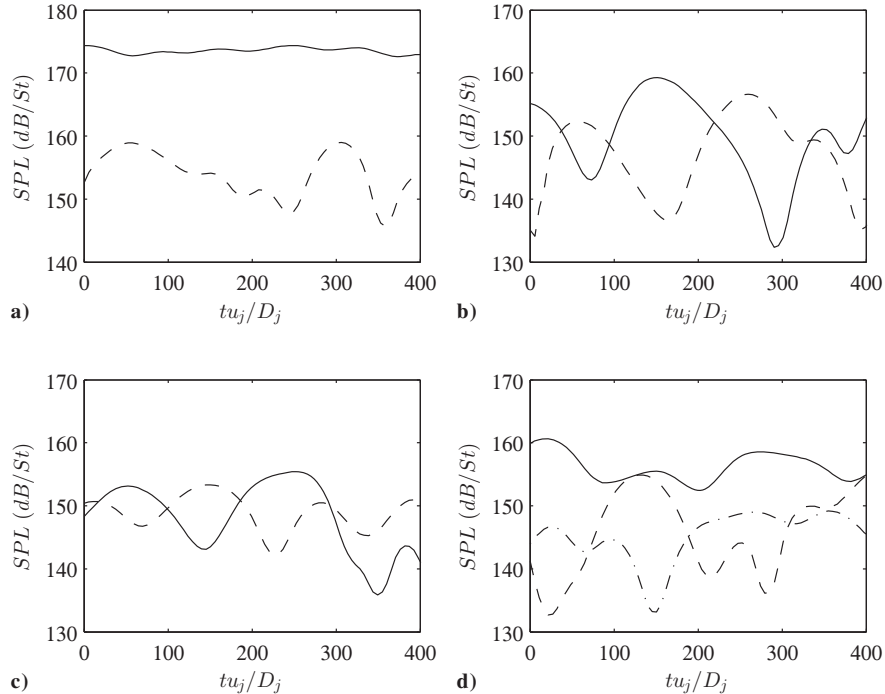

Fig. 23 Sound pressure levels obtained at $r = D$ and $z = 0$ as a function of time for a) JetL2.1, b) JetL2.8, c) JetL3.6, and d) JetL4.7 at St_1 (dashed line), St_2 (solid line), and St_3 (dash-dotted line).

switch seems to be observed between the two tones at $St_1 = 0.345$ and $St_2 = 0.42$. For JetL4.7, as noted previously, the amplitude of the dominant tone at $St_2 = 0.34$ does not change much and only varies between 153 and 161 dB/St, whereas those of the tones at $St_1 = 0.27$ and $St_3 = 0.42$ oscillate between 133 and 155 dB/St and between 134 and 148 dB/St, respectively.

Finally, it can be noted that the tone intensities significantly vary in time in all cases except for the two cases where the near-wall Mach disk has a nearly periodic motion at the dominant tone frequency, namely an axially pulsing motion at $St_2 = 0.505$ in JetL2.1 and a helical motion at $St_2 = 0.34$ in JetL4.7.

IV. Conclusions

In this paper, the flow and near pressure fields of an underexpanded jet at a fully expanded Mach number of 1.56 and a Reynolds number of 6×10^4 impinging on a flat plate at four distances between 2.08 and 4.66 nozzle-exit diameters have been presented. Overall, the results compare well with experimental data of the literature for jets with similar initial conditions. This is particularly the case for the frequencies of the acoustic tones generated by the feedback mechanism establishing between the jet nozzle and the flat plate. The tone frequencies are also roughly predicted by the usual expression derived for an aeroacoustic feedback loop, regardless of the

formation of a Mach disk in the jet close to the flat plate. On the contrary, the intensities of the tones are stronger in the case where such a Mach disk is present than in the case without Mach disk, in agreement with experimental observations. Moreover, using Fourier decomposition of the pressure field, it appears that the oscillation modes obtained for the different tone frequencies are helical, with the exception of that for the dominant tone frequency in the case with the smallest nozzle-to-plate distance L/D, which is axisymmetric.

In the three cases where there is a Mach disk in the jet just upstream from the flat plate, the motions of the Mach disk have been investigated. As in experiments, two kinds of motions, namely an axially pulsing mode for $L/D = 2.08D$ and a helical impinging mode for $L/D = 2.8D$ and $L/D = 4.66D$, are observed. They occur at the same frequency and have the same axisymmetric or helical nature as the dominant tone of the feedback mechanism. Finally, the Mach disk motions also seem to be correlated with the tone intermittency. The tone intensities are indeed found to significantly vary in time except when the near-wall Mach disk has a nearly periodic motion at the tone frequency.

References

[1] Powell, A., "On Edge Tones and Associated Phenomena," *Acta Acustica United with Acustica*, Vol. 3, 1953, pp. 233–243.

[2] Wagner, F. R., "The Sound and Flow Field of an Axially Symmetric Free Jet upon Impact on a Wall," NASA Rept. TT F-13942, 1971.

[3] Rockwell, D., and Naudascher, E., "Self-Sustained Oscillations of Impinging Free Shear Layers," *Annual Review of Fluid Mechanics*, Vol. 11, 1979, pp. 67–94.
doi:10.1146/annurev.fl.11.010179.000435

[4] Rockwell, D., "Oscillations of Impinging Shear Layers," *AIAA Journal*, Vol. 21, No. 5, 1983, pp. 645–664.
doi:10.2514/3.8130

[5] Ho, C. M., and Nosseir, N. S., "Dynamics of an Impinging Jet. Part 1. The feedback Phenomenon," *Journal of Fluid Mechanics*, Vol. 105, April 1981, pp. 119–142.
doi:10.1017/S0022112081003133

[6] Nosseir, N. S., and Ho, C. M., "Dynamics of an Impinging Jet. Part 2. The Noise Generation," *Journal of Fluid Mechanics*, Vol. 116, March 1982, pp. 379–391.
doi:10.1017/S0022112082000512

[7] Tam, C. K. W., and Ahuja, K. K., "Theoretical Model of Discrete Tone Generation by Impinging Jets," *Journal of Fluid Mechanics*, Vol. 214, May 1990, pp. 67–87.
doi:10.1017/S0022112090000052

[8] Henderson, B., and Powell, A., "Experiments Concerning Tones Produced by an Axisymmetric Choked Jet Impinging on Flat Plates," *Journal of Sound Vibration*, Vol. 168, No. 2, 1993, pp. 307–326.
doi:10.1006/jsvi.1993.1375

[9] Krothapalli, A., Rajkuperan, E., Alvi, F., and Lourenco, L., "Flow Field and Noise Characteristics of a Supersonic Impinging Jet," *Journal of Fluid Mechanics*, Vol. 392, Aug. 1999, pp. 155–181.
doi:10.1017/S0022112099005406

[10] Henderson, B., Bridges, J., and Wernet, M., "An Experimental Study of the Oscillatory Flow Structure of Tone-Producing Supersonic Impinging Jets," *Journal of Fluid Mechanics*, Vol. 542, Nov. 2005, pp. 115–126.
doi:10.1017/S0022112005006385

[11] Risborg, A., and Soria, J., "High-Speed Optical Measurements of an Underexpanded Supersonic Jet Impinging on an Inclined Plate," *Proceedings of the 28th International Congress on High-Speed Imaging and Photonics*, Vol. 7126, 2009.

[12] Buchmann, N. A., Mitchell, D. M., Ingvorsen, K. M., Honnery, D. R., and Soria, J., "High Spatial Resolution Imaging of a Supersonic Underexpanded Jet Impinging on a Flat Plate," *Proceedings the 6th Australian Conference on Laser Diagnostics in Fluid Mechanics and Combustion*, Vol. 116, 2011.

[13] Mitchell, D. M., Honnery, D. R., and Soria, J., "The Visualization of the Acoustic Feedback Loop in Impinging Underexpanded Supersonic Jet Flows Using Ultra-High Frame Rate Schlieren," *Journal of Visualization*, Vol. 15, No. 4, 2012, pp. 333–341.
doi:10.1007/s12650-012-0139-9

[14] Uzun, A., Kumar, R., Hussaini, M. Y., and Alvi, F. S., "Simulation of Tonal Noise Generation by Supersonic Impinging Jets," *AIAA Journal*, Vol. 51, No. 7, 2013, pp. 1593–1611.
doi:10.2514/1.J051839

[15] Kuo, C. Y., and Dowling, A. P., "Oscillations of a Moderately Underexpanded Choked Jet Impinging Upon a Flat Plate," *Journal of Fluid Mechanics*, Vol. 315, May 1996, pp. 267–291.

[16] Powell, A., "The Sound-Producing Oscillations of Round Underexpanded Jets Impinging on Normal Plates," *Journal of the Acoustical Society of America*, Vol. 83, No. 2, 1988, pp. 515–533.
doi:10.1121/1.396146

[17] Dauptain, A., Cuenot, B., and Gicquel, L. Y. M., "Large Eddy Simulation of Stable Supersonic Jet Impinging on Flat Plate," *AIAA Journal*, Vol. 48, No. 10, 2010, pp. 2325–2338.
doi:10.2514/1.J050362

[18] Dauptain, A., Gicquel, L. Y. M., and Moreau, S., "Large Eddy Simulation of Supersonic Impinging Jets," *AIAA Journal*, Vol. 50, No. 7, 2012, pp. 1560–1574.
doi:10.2514/1.J051470

[19] Bogey, C., Marsden, O., and Bailly, C., "Large-Eddy Simulation of the Flow and Acoustic Fields of a Reynolds Number 10^5 Subsonic Jet with Tripped Exit Boundary Layers," *Physics of Fluids*, Vol. 23, No. 3, 2011, Paper 035104.

[20] Bogey, C., and Bailly, C., "A Family of Low Dispersive and Low Dissipative Explicit Schemes for Flow and Noise Computations," *Journal of Computational Physics*, Vol. 194, No. 1, 2004, pp. 194–214.
doi:10.1016/j.jcp.2003.09.003

[21] Berland, J., Bogey, C., Marsden, O., and Bailly, C., "High-Order, Low Dispersive and Low Dissipative Explicit Schemes for Multiple-Scale and Boundary Problems," *Journal of Computational Physics*, Vol. 224, No. 2, 2007, pp. 637–662.
doi:10.1016/j.jcp.2006.10.017

[22] Bogey, C., de Cacqueray, N., and Bailly, C., "A Shock-Capturing Methodology Based on Adaptive Spatial Filtering for High-Order Non-Linear Computations," *Journal of Computational Physics*, Vol. 228, 2009, pp. 1447–1465.
doi:10.1016/j.jcp.2008.10.042

[23] Bogey, C., and Bailly, C., "Large Eddy Simulations of Transitional Round Jets: Influence of the Reynolds Number on Flow Development and Energy Dissipation," *Physics of Fluids*, Vol. 18, No. 6, 2006, Paper 065101.

[24] Bogey, C., and Bailly, C., "Turbulence and Energy Budget in a Self-Preserving Round Jet: Direct Evaluation Using Large Eddy Simulation," *Journal of Fluid Mechanics*, Vol. 627, May 2009, pp. 129–160.
doi:10.1017/S0022112009005801

[25] Fauconnier, D., Bogey, C., and Dick, E., "On the Performance of Relaxation Filtering for Large-Eddy Simulation," *Journal of Turbulence*, Vol. 14, No. 1, 2013, pp. 22–49.
doi:10.1080/14685248.2012.740567

[26] Kremer, F., and Bogey, C., "Large-Eddy Simulation of Turbulent Channel Flow Using Relaxation Filtering: Resolution Requirement and Reynolds Number Effects," *Computers & Fluids*, Vol. 116, 2015, pp. 17–28.
doi:10.1016/j.compfluid.2015.03.026

[27] Tam, C. K. W., and Dong, Z., "Wall Boundary Conditions for High-Order Finite-Difference Schemes in Computational Aeroacoustics," *Theoretical and Computational Fluid Dynamics*, Vol. 6, 1994, pp. 303–322.
doi:10.1007/BF00311843

[28] Mohseni, K., and Colonius, T., "Numerical Treatment of Polar Coordinate Singularities," *Journal of Computational Physics*, Vol. 157, No. 2, 2000, pp. 787–795.
doi:10.1006/jcph.1999.6382

[29] Bogey, C., de Cacqueray, N., and Bailly, C., "Finite Differences for Coarse Azimuthal Discretization and for Reduction of Effective Resolution near Origin of Cylindrical Flow Equations," *Journal of Computational Physics*, Vol. 230, No. 4, 2011, pp. 1134–1146.
doi:10.1016/j.jcp.2010.10.031

[30] Bogey, C., Marsden, O., and Bailly, C., "Influence of Initial Turbulence Level on the Flow and Sound Fields of a Subsonic Jet at a Diameter-Based Reynolds Number of 10^5," *Journal of Fluid Mechanics*, Vol. 701, June 2012, pp. 352–385.
doi:10.1017/jfm.2012.162

[31] Bogey, C., Marsden, O., and Bailly, C., "Effects of Moderate Reynolds Numbers on Subsonic Round Jets with Highly Disturbed Nozzle-Exit Boundary Layers," *Physics of Fluids*, Vol. 24, No. 10, 2012, Paper 105107.
doi:10.1063/1.4757667

[32] Bogey, C., and Marsden, O., "Simulations of Initially Highly Disturbed Jets with Experiment-Like Exit Boundary Layers," *AIAA Journal*, Vol. 54, No. 4, 2016, pp. 1299–1312.
doi:10.2514/1.J054426

[33] de Cacqueray, N., Bogey, C., and Bailly, C., "Investigation of a High-Mach-Number Overexpanded Jet Using Large-Eddy Simulation," *AIAA Journal*, Vol. 49, No. 10, 2011, pp. 2171–2182.
doi:10.2514/1.J050952

[34] Viazzo, S., Dejoan, A., and Schiestel, R., "Spectral Features of the Wall-Pressure Fluctuations in Turbulent Wall Flows with and Without Perturbations Using LES," *International Journal of Heat Fluid Flow*, Vol. 22, No. 1, 2001, pp. 39–52.
doi:10.1016/S0142-727X(00)00074-6

[35] Gloerfelt, X., and Berland, J., "Direct Computation of Turbulent Boundary Layer Noise," *15th AIAA/CEAS Aeroacoustics Conference*, AIAA Paper 2009-3401, May 2009.

[36] Schlatter, P., Li, Q., Brethouwer, G., Johansson, A. V., and Henningson, D. S., "Simulations of Spatially Evolving Turbulent Boundary Layers up to $Re_\theta = 4300$," *International Journal of Heat Fluid Flow*, Vol. 31, No. 3, 2010, pp. 251–261.
doi:10.1016/j.ijheatfluidflow.2009.12.011

[37] Gojon, R., Bogey, C., and Marsden, O., "Large-Eddy Simulation of Underexpanded Round Jets Impinging on a Flat Plate 4 to 9 Radii Downstream from the Nozzle," *21st AIAA/CEAS Aeroacoustics Conference*, AIAA Paper 2015-2210, 2015.

[38] Arnette, S. A., Samimy, M., and Elliott, G. S., "On Streamwise Vortices in High Reynolds Number Supersonic Axisymmetric Jets," *Physics of Fluids*, Vol. 5, No. 1, 1993, pp. 187–202.
doi:10.1063/1.858803

[39] André, B., "Etude Expérimentale de l'Effet du Vol sur le Bruit de Choc de Jets Supersoniques Sous-Détendus," Ph.D. Dissertation, École Centrale de Lyon, Écully, France, 2012.

[40] Harper-Bourne, M., and Fisher, M. J., "The Noise from Shock in Supersonic Jets," *Proceedings of the AGARD Conference on Noise Mechanisms*, AGARD-CP-131, 1973, pp. 1–11.

[41] Henderson, B., "The Connection Between Sound Production and Jet Structure of the Supersonic Impinging Jet," *Journal of the Acoustical Society of America*, Vol. 111, No. 2, 2002, pp. 735–747.
doi:10.1121/1.1436069

[42] Gojon, R., and Bogey, C., "Azimuthal Organisation of Turbulent Structures in Underexpanded Impinging Round Jets," *22nd AIAA/CEAS Aeroacoustics Conference*, AIAA Paper 2016-2929, 2016.

[43] Gojon, R., Bogey, C., and Marsden, O., "Investigation of Tone Generation in Ideally Expanded Supersonic Planar Impinging Jets Using Large-Eddy Simulation," *Journal of Fluid Mechanics*, Vol. 808, Dec. 2016, pp. 90–115.
doi:10.1017/jfm.2016.628

D. Papamoschou
Associate Editor